Journal of Fluids and Structures 39 (2013) 237–257

Contents lists available at SciVerse ScienceDirect

Journal of Fluids and Structures

journal homepage: www.elsevier.com/locate/jfs

Two-degree-of-freedom vortex-induced vibration of circular cylinders with very low aspect ratio and small mass ratio

R.T. Gonçalves [a,*], G.F. Rosetti [a], G.R. Franzini [b], J.R. Meneghini [b], A.L.C. Fujarra [a,1]

[a] TPN, Department of Naval Architecture and Ocean Engineering, Escola Politécnica, University of São Paulo, Av. Prof. Mello Moraes, 2231, Cidade Universitária, São Paulo, SP 05508-030, Brazil

[b] NDF, Department of Mechanical Engineering, Escola Politécnica, University of São Paulo, Av. Prof. Mello Moraes, 2231, Cidade Universitária, São Paulo, SP 05508-030, Brazil

ARTICLE INFO

Article history:
Received 16 March 2012
Accepted 3 February 2013
Available online 1 April 2013

Keywords:
Vortex-induced vibration
Very low aspect ratio
Small mass ratio
Two degrees of freedom
Circular cylinders

ABSTRACT

The investigation of vortex-induced vibration on very short cylinders with two degrees of freedom has drawn the attention of a large number of researchers. Some investigations on such a problem are carried out in order to have a better understanding of the physics involved in vortex-induced motions of floating bodies such as offshore platforms. In this paper, experiments were carried out in a recirculating water channel over the range of Reynolds number $6000 < Re < 70\,000$. Measured response amplitudes and frequencies of cylinders with two degrees of freedom, three different small mass ratios ($m^*=1.00$; 2.62 and 4.36) and very low aspect ratios ($0.3 \le L/D \le 2.0$) were shown and the results were discussed in depth. Conversely to what would be expected for cylinders with very low aspect ratio, the results showed large motions in the transverse direction with maximum amplitudes around 1.5 diameters for cylinders with $L/D=2.0$, despite being smaller when the aspect ratio is reduced. Moreover, the response amplitudes presented high values around 0.4 diameters in the in-line direction. In fact, the large transverse motions were related to a strong coupling with the in-line responses, visibly identified in the plots of nondimensional frequency, as well as by the trajectories in the *XY*-plane, *Lissajous* figures, particularly in the case of $m^*=1.00$ and $L/D=2.0$, when *8-shape* trajectories were clearly observed. The case of $m^*=1.00$ deserves more attention because of its smaller amplitude compared to the cases with the same aspect ratio and a larger mass ratio. This counter-intuitive behavior seems to be related to the energy transferring process from the steady stream to the oscillatory hydroelastic system. Finally, it is noteworthy that the characteristic of the "Strouhal-like" number decreases when the aspect ratio decreases, as also observed in previous works available in the literature, most of them for stationary cylinders.

1. Introduction

Some floating systems for deep sea oil and gas production have shown high susceptibility to the vortex-induced motion (VIM), a resonant phenomenon essentially distinguished by its large amplitude and low frequency of oscillation at the free

* Corresponding author. Tel.: +55 11 30915341.
E-mail address: rodolfo_tg@tpn.usp.br (R.T. Gonçalves).

[1] Visiting researcher at the Maritime Research Institute Netherlands—MARIN, Wageningen, The Netherlands.

0889-9746/$ - see front matter
http://dx.doi.org/10.1016/j.jfluidstructs.2013.02.004

Nomenclature

γ	modal form factor
ζ_s	structural damping
ζ_w	damping coefficient in still water
ρ	water density
$A_x/(\gamma D)$	characteristic nondimensional motion amplitude in the in-line direction
$A_y/(\gamma D)$	characteristic nondimensional motion amplitude in the transverse direction
D	characteristic diameter
D_1	run-up of the water on the front of the cylinder
Fr_L	Froude number based on submerged cylinder length
f_0	natural frequency in still water, both in in-line and transverse directions
f_{0x}	natural frequency of the system in still water at the in-line direction
f_{0y}	natural frequency of the system in still water at the transverse direction
f_s	vortex-shedding frequency
f_x	oscillation frequency in the in-line direction
f_y	oscillation frequency in the transverse direction
L	immersed length
L_0	water elevation behind the cylinder
m^*	mass ratio
m_{ax}	added mass in the in-line direction
m^*_{ax}	added mass coefficient in the in-line direction
m_{ay}	added mass in the transverse direction
m^*_{ay}	added mass coefficient in the transverse direction
m_d	displaced mass
m_s	structural mass
$L\,/\,D$	aspect ratio
Re	Reynolds number
T	kinetic energy of the oscillatory system
U	flow velocity
U_x	component of the cylinder velocity in the in-line direction
U_y	component of the cylinder velocity in the transverse direction
V_r	reduced velocity
V_x	nondimensional velocity in the in-line direction
V_x	nondimensional velocity in the transverse direction
X	in-line direction
Y	transverse direction

surface plane due to current incidences. A little more than one decade since research started, it is known that VIM presents a dynamic behavior similar to the vortex-induced vibration (VIV) phenomenon, usually acting on slender structures free to oscillate under fluid flow. However, despite similarities in the global behavior, there are some differences comparing the phenomenological characteristics of VIM to the classical VIV, mainly considering two important characteristics of the system, which are its immersed length and number of degrees of freedom in the fluid flow. In the case of floating bodies, such as offshore platforms, it is worth highlighting the relevance of all degrees of freedom to the system dynamics, as well as the enormous amount of tridimensional effects present in the wake.

Looking for investigations into the influence of the cylinder length on the VIV phenomenon, scientifically recognized by the influence of the aspect ratio parameter for circular cylinders, i.e. the ratio between length and diameter, L/D, one will realize that most of the available studies are related to fixed cylinders under the effects of a free end. Concomitantly, by performing a second search for the influence of the number of degrees of freedom on the VIV, the already known coexistence between transverse and in-line oscillations, the same researcher will find a vast majority of works discussing the dynamic of flexible cylinders and/or rigid ones elastically supported with one or two degrees of freedom, but in both cases always characterized by high aspect ratio.

Considering this scenario, it is possible to point out the exact purpose for the present work, namely to investigate the VIV phenomenon on rigid cylinders with very low aspect ratio, $0.3 < L/D < 2.0$, subjected to strong free-end effects and, at the same time, presenting small values of mass ratio and two degrees of freedom, i.e. transverse and in-line to the fluid flow, from now on simply referred to as 2-dof. By means of experiments in a recirculating water channel, the ultimate goal is to collect fundamental aspects for better understanding the dynamic behavior presented by the VIM phenomenon. Obviously, it is important to emphasize that the present work is far from being conclusive but, even with the limited scope presented further on, provides advances related to the VIV phenomenon on short cylinders with small mass ratio and 2-dof under a range of reduced velocity, $2 < V_r < 12$, at least to our knowledge, unprecedented experimental results in the literature.

Before the presentation of the experiments, it is important to review the main effects of the low aspect ratio and the 2-dof on the VIV phenomenon of circular cylinders, remarking that the results presented herein were achieved through the surveys mentioned above, in which most results found do not consider both issues together, therefore being impossible to apply them directly to the proposed problem.

Starting from the survey concerning the aspect ratio, it is known that two major controversial issues are related to its influence on the VIV phenomenon, namely the flow around the finite cylinders and what kind of vortical structure is found close to the free end. As originally discussed in Okamoto and Yagita (1973), it is widely accepted that the vortex shedding decreases as the aspect ratio is decreased. It is also known that the flow configuration downstream of a rigid and fixed cylinder depends on the aspect ratio, and that it is possible to define a critical value of $L/D \cong 2.0$, in which changes occur in the flow pattern configuration, as proposed by Sakamoto and Arie (1983). In fact, taking into account this critical value of aspect ratio, in Kawamura et al. (1984) two flow pattern configurations around the finite cylinder are presented. For aspect ratios above the critical value, the existence of a *von Kármán* vortex shedding just below the region affected by the downwash effect promoted by the trailing vortices near the free end is proposed. On the other hand, for aspect ratios below the critical value, another configuration where the *von Kármán* vortex shedding ceases to exist is proposed.

At this point, the first divergence arises, particularly concerning the existence, or not, of the trailing vortices at the free end of the fixed cylinder. In Okamoto and Yagita (1973), for example, instead of the trailing vortices, a gradual delay on the *von Kármán* vortex shedding near the free end is suggested, causing a continuous line of vortices properly inclined and attached to the free end. Additionally, Sakamoto and Arie (1983) have suggested that an *arch-type* shedding takes place instead of the *von Kármán* vortex shedding for a cylinder with aspect ratio below the critical value. On the other hand, more recent studies, such as Adaramola et al. (2006), Park and Lee (2000), Rödiger et al. (2007), Roh and Park (2003), Rostamy et al. (2012) and Sumner et al. (2004) provided strong evidence for the trailing vortices, yet without a topological explanation for their interaction with the *von Kármán* vortex shedding at a near distance from the tip. Moreover, in Roh and Park (2003), a vortical structure comprising two pairs of counter-rotating vortices at the free end of the rigid and fixed cylinder is proposed, accounting for the downwash effect on the wake. Details about the topological interaction between the trailing vortices and the *von Kármán* wake can be found in Palau-Salvador et al. (2010), recently obtained by using a combination of experiments and Large Eddy Simulation (LES) for cylinders with $L/D = 2.0$ and 5.0.

Regardless of the vortical structure, it is quite clear that those flow pattern configurations around finite cylinders are responsible for the changes in the Strouhal number along the cylinder. However, a doubt about how it happens still persists. According to researches, based on measurements of the velocity field near the fixed cylinder, such as those found in Okamoto and Yagita (1973), it was proposed to be a gradual decrease of the Strouhal number towards the tip, with lower values found between 2 and 4 diameters from there and with null values for distances smaller than 2 diameters. Actually, in Ayoub and Karamcheti (1982) an unstable and intermittent vortex shedding process inside this latter region was suggested, making it difficult to define a Strouhal number for this case. Among recent studies, force measurements in Baban and So (1991a, 1991b) and Iungo et al. (2012), for cylinders with $L/D \leq 3.00$, confirmed a fluctuating lift induced by alternating vortex shedding, and St lower than the high aspect ratio cylinders. Conversely, investigations based on the pressure measurements on the fixed cylinder surface and also by means of the fluctuations in the lift force, as those found in Farivar (1981), Fox and West (1993a, 1993b) and Fox and Apelt (1993) reported a Strouhal number varying in steps toward the tip as a consequence of a cellular structure in the vortex shedding.

Another important issue in our experiments is that the cylinder pierces the free surface. This fact changes the pressures around the cylinder with the Froude numbers increases, as observed in Sarpkaya (1996). Hay (1947) performed a series of tests with a vertical surface-piercing cylinder of various diameters and submerged length to measure total mean resistance and mean water surface elevations. In that work, Hay performed tests to show the extent D_1 of the run-up on the centre-line on the front of the cylinder, and of the depression L_0 of the maximum draw-down on the centre-line in the rear, in function of Fr_L, where $\mathrm{Fr}_L = U/\sqrt{gL}$ is the Froude number based on the cylinder submerged length L. This definition is more indicated for cylinders with low aspect ratio and with free end as also confirmed by Chaplin and Teigen (2003). In the work by Chaplin and Teigen (2003), Hay's experiments were revisited and compared with results for cylinders considered infinite. The two approximations obtained by Hay's experiments, the first one for the maximum depression L_0 of the water behind the cylinder (as $L_0/D = 0.286\,{\mathrm{Fr}_L}^2$) and the second one for the maximum run-up D_1 of the water on the front of the cylinder (as $D_1/D = {\mathrm{Fr}_L}^2/2$) were confirmed by Chaplin and Teigen (2003). The authors showed a great increase in the surface resistance force for $\mathrm{Fr}_L > 0.5$ with maximum value at $\mathrm{Fr}_L = 1$ and decrease after this. This information will be used further in the results presented in this paper to try to understand the free surface effect on the VIV of very low aspect ratio cylinders.

To our knowledge, only three experimental works considering both issues, free-end effects and 2-dof, simultaneously have been found, even so recently. In Nakamura et al. (2001), only vibrations in the flow direction were investigated as a function of the aspect ratio of a rigid cylinder elastically supported ($5.0 < L/D < 21.0$). According to the experimental results in a water tunnel, the aspect ratio changes the transition between the resonant regions in the flow direction (from the *SS—Streamwise Symmetric* to the *AS—Streamwise Antisymmetric* vortex shedding, originally described in King (1974)), but it does not change the maximum amplitude of oscillation. Furthermore, in Morse et al. (2008), the free-end effect was investigated by considering a rigid cylinder elastically supported with $L/D = 8.0$ and free to oscillate only in the transverse direction to the flow. Against expectation, the transverse amplitudes of oscillation for the cylinder equipped with an endplate were no higher than those presented by the same cylinder without it. Aside from those works, in Someya et al. (2010), the first results of the VIV phenomenon are found acting on a cylinder with low aspect ratio and 2-dof but, unfortunately, only for reduced velocities up to 4. Despite that, some evidence is given that cylinders presenting 2-dof can keep the vortex shedding even for a lower aspect ratio, responsible for a behavior very similar to that usually found for long cylinders.

Bearing in mind that 2-dof have shown to be important for better understanding the VIV phenomenon, by performing a second survey concerning the coexistence between in-line and transverse oscillations, one realizes that other aspects also have to be considered. Cylinders free to oscillate with 2-dof present the possibility of coupled movements in *8-shape* like those *Lissajous* figures reported, for example, in Pesce and Fujarra (2000) and described in Jauvtis and Williamson (2003) and Williamson and Jauvtis (2004). According to Williamson and his co-author, the *8-shape* movements can result from a periodic vortex wake mode comprising a triplet of vortices being formed in each half cycle, the so-called "2T" mode and being present in systems with mass ratio lower than 6.0. It is worth mentioning that the *8*-shape movements are not unique to the "2T" wake mode, since *8*-shape movements have been observed by Dahl et al. (2007) even when a "2T" mode is not present. Additionally, in Jauvtis and Williamson (2004) a critical value was defined for the mass ratio, $m^*_{critical} = 0.52$, below which the lower branch is not present within the synchronization region. After that, in Stappenbelt and Lalji (2008), the critical mass-damping, $(m^*\zeta_s)_{crit} = 0.066$, was presented as a more suitable parameter to state the possibility of coupled oscillations between transverse and in-line directions, a suggestion confirmed in Sanchis et al. (2008). Furthermore, in Sanchis (2009), the coupled movement was studied as a function of the relation between the natural frequencies of the system in still water at the in-line and transverse direction, f_{0x}/f_{0y}, confirming the existence of changes due to the relative phase between movements in those degrees of freedom. Such changes have already been reported in Dahl et al. (2007).

A precise relationship between the VIV response and changes of parameters such as mass ratio, damping coefficient and Reynolds number can be found in Blevins and Coughran (2009), comprising experiments with cylinders free to oscillate in 1-dof and 2-dof, with mass ratio varying in the range $1.0 \le m^* \le 11.0$ and damping coefficient in the range of $0.002 \le \zeta_s \le 0.400$, as well as reduced velocities ranging from $2 < V_r < 12$ and Reynolds numbers up to 1.5×10^5. The main results were as follows. Firstly, by increasing the damping coefficient for a mass ratio fixed in $m^* = 3.2$, smaller oscillations in the transverse direction were observed for higher damping levels, presenting maximum values of amplitude in gradually lower reduced velocities. A second set of experiments was performed by considering a fixed damping coefficient in $\zeta = 0.020$ and different values of mass ratio. The results for $m^* > 1.0$ were quite similar to those discussed by Jauvtis and Williamson (2004), particularly concerning the qualitative response of VIV, which means that the presence of both branches for responses associated to the longitudinal oscillations at $2 \le V_r \le 4$, i.e. *SS—Streamwise Symmetric* and *AS—Streamwise Antisymmetric*, as well as all the branches coming from the transversal oscillations due to reduced velocities up to approximately 12, i.e. the branches *I—Initial*, *U—Upper* and *L—Lower*. Likewise, Williamson and Jauvtis, Blevins and Coughran also recognized a branch of coupled movements in *8-shape* and high amplitudes in the transverse direction, although with no mention to the pattern of shedding responsible for it. Also, for each increase in the mass ratio, the coupled movements have ceased to exist at lower values of reduced velocity. Conversely, by decreasing the mass ratio, the initial branch appeared gradually at lower reduced velocities. Finally, the results for $m^* = 1.0$, $\zeta = 0.063$, $L/D > 13.0$ and 2-dof performed by those authors are the first in the literature for a large range of reduced velocities. Although not conclusive, a continuous increase of the transversal oscillation was pointed out with no evidence of the lower branch, the same behavior proposed in Stappenbelt and Lalji (2008) by means of the critical value of the mass-damping parameter and quite close to the response recognized for the VIM measured in small-scale experiments of platforms.

According to the aspects described so far, by conducting experiments addressing the influence of the aspect ratio on the VIV of circular cylinders with 2-dof and small values of mass ratio, it is possible to infer their relevance for understanding the VIM phenomenon in a fundamental stage, main objective of the present work.

2. Experimental set-up

The experiments herein presented were carried out in the recirculating water channel available at NDF (Fluid and Dynamics Research Group) of the University of São Paulo, Brazil, presenting a section of $0.70 \times 0.80 \times 7.50$ m^3 for tests and around 3% of turbulence operating with free-stream velocities up to $U = 0.70$ m/s. Additional details concerning this facility can be found in Assi et al. (2006).

By means of a rigid cylinder elastically supported by a cantilevered beam, previously described in Franzini et al. (2010) and Gonçalves et al. (2010a), tests were performed up to velocities of approximately 0.40 m/s. As shown in Fig. 1, the vertical cylinder with 125 mm in diameter was kept free to oscillate transverse and in-line to the fluid flow, presenting the same natural frequency in both directions. The structural damping coefficient was very low, approximately $\zeta_s = 0.1\%$, measured through free-decaying tests conducted in air. The stiffness of the elastic support was defined by the length of the cantilevered beam, the velocities carried out correspond to a range of Reynolds numbers from 6000 to 70 000.

Seven different values of aspect ratio ranging from 0.30 to 2.00 were tested by changing the water level of the channel. Moreover, three values of the mass ratio parameter were considered, namely $m^* = 4m_s/\rho\pi D^2 L = 1.00$, 2.62 and 4.36 (where m_s is the oscillating structural mass); the alteration in mass ratios was made by changing the mass inside the cylinder using ballast. The natural frequency in still water depends on the aspect ratio and mass ratio consequently.

Table 1 presents all the parameters for the tests, including the damping coefficient in still water, ζ_w, and the natural frequency in still water. The natural frequencies are the same in the transverse and in-line directions, $f_{0x} = f_{0y} = f_0$ for each condition tested.

The Froude number of the tests were defined as a function of the flow velocity and the cylinder submerged length as $\mathrm{Fr}_L = U/\sqrt{gL}$. As can be seen in Table 1, only few cases have $\mathrm{Fr}_L > 0.5$ for the highest reduced velocities. For this particular condition, $L/D < 1.0$, the free-surface effects are large and can introduce more tridimensional effects in the flow, but these effects could not be detached from the free-end effects.

For very low aspect ratio, $L/D < 1.0$, the drift is very small and so is the inclination of the cylinder. The drift caused by the drag for higher aspect ratio cases, $L/D > 1.0$, can bring about inclination of the cylinder up to 5°. Even for these cases, the effect of the inclination can be neglected.

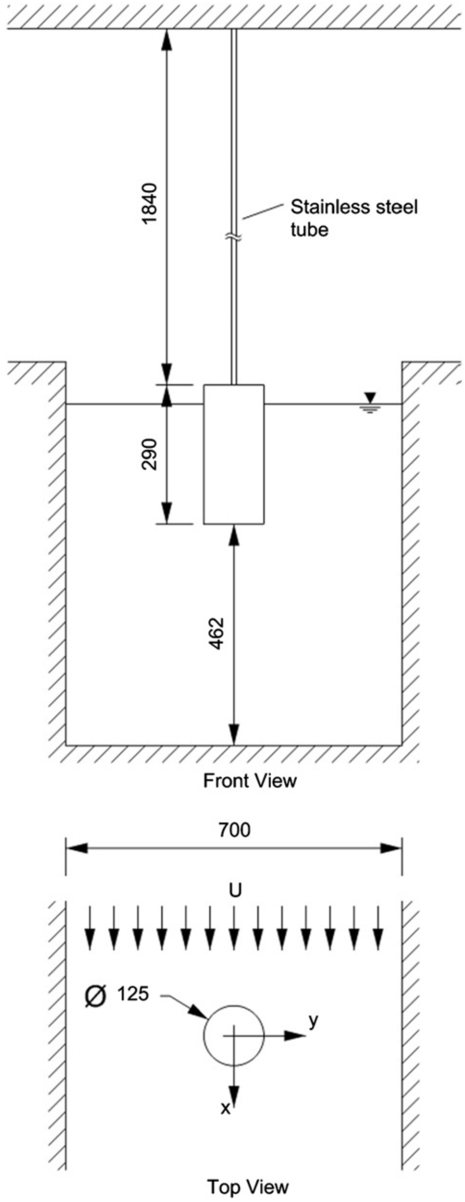

Fig. 1. Experimental setup showing the rigid cylinder elastically supported by a cantilevered beam.

Forces were not measured in the tests, nor was the vortex-shedding frequency. The "Strouhal-like" numbers were calculated as the inclination of the curve f_y/f_0 outside the lock-in range, assuming that the vortex-shedding frequency is the same of the transverse motions, i.e., $f_s = f_y$.

In terms of the data acquisition procedure, all the time histories of displacement were obtained by using two laser position sensors, considering at least 30 cycles in steady state. The flow velocities were set by steps with 120 s between them in order to avoid transient effects due to the flow acceleration and, therefore, assuring enough time for stabilizing the flow velocities.

3. Method of analysis

The nondimensional displacements presented later in this work were considered at the tip of the setup illustrated in Fig. 1, which means the free end of the short cylinder. In order to compare these displacements with those from different experimental facilities, a modal form factor γ_n is appropriate, as presented, for example, in Blevins (1990) and also used in Gonçalves et al. (2012b).

Table 1
Parameters of the tests performed.

m^*	L/D	Re	ζ_w (%)	f_0 (Hz)	Fr_L
4.36	2.00	13 600–50 000	2.28	0.30	0.07–0.26
	1.50	11 500–53 500	2.70	0.31	0.07–0.32
	1.00	17 100–55 800	3.62	0.34	0.12–0.40
	0.75	10 400–56 900	3.77	0.36	0.09–0.47
	0.50	8700–61 500	4.09	0.40	0.09–0.63
	0.40	17 100–64 800	4.38	0.44	0.20–0.74
	0.30	17 600–67 900	4.46	0.48	0.23–0.90
2.62	2.00	13 600–49 300	2.73	0.27	0.07–0.25
	1.00	12 000–55 800	4.00	0.32	0.09–0.40
	0.75	10 100–57 100	4.85	0.35	0.08–0.48
	0.50	16 900–59 400	5.11	0.41	0.17–0.61
1.00	2.00	6600–27 800	3.98	0.16	0.03–0.14
	1.50	6000–39 400	4.86	0.21	0.04–0.23

In sum, the modal form factor is a way of considering the characteristic of the natural vibration of the support structure, allowing displacements in any location to be properly compared to the translational movement of a rigid structure, for instance, a cylinder elastically supported. In this case, calculating the modal form factor for the cantilevered beam, one can achieve $\gamma_{n=1}=1.305$. For the sake of conciseness, as this work will present results only for the first mode of vibration, the nomenclature $\gamma=1.305$ will be adopted.

In terms of signal processing, the experimental results of VIV on the low aspect ratio cylinders were analyzed by means of the Hilbert–Huang Transform Method (HHT). Its application on VIV results was first presented in Pesce et al. (2006), followed by a series of publications, such as those by Franzini et al. (2008, 2011), Gonçalves et al. (2012a, 2012b) and Silveira et al. (2007).

The HHT was developed in Huang et al. (1998) as an alternative to deal with non-stationary signals that arise from non-linear systems. The nondimensional amplitude was defined by taking the mean of the 10% largest amplitudes obtained in the HHT, both for motion in the transverse and in-line directions. It is important to highlight that in the HHT there are instantaneous amplitudes of displacement, so the number of points to calculate the mean of the 10% largest amplitudes is proportional to the length of data and, consequently, to the sampling frequency, which implies a reduction in the statistic uncertainty; see details in Gonçalves et al. (2012a). On the other hand, using the traditional 10% largest peak amplitudes, there are few points comparing to the HHT.

4. Experimental results

The results from the experiments performed considering cylinders with small mass ratio and low aspect ratio are presented in the next subsections, comprising nondimensional amplitudes and frequencies in both transverse and in-line direction as a function of the reduced velocity, $V_r = U/f_0 D$, as well as the time traces of movement (*Lissajous* figures) for supporting the discussions and conclusions.

4.1. The response for fixed mass ratio and different aspect ratios

Figs. 2 and 3, respectively, show the transverse and in-line nondimensional amplitudes for the case of $m^*=4.36$ and $L/D=0.3,0.4,0.5,0.75,1.0,1.5$ and 2.0. Additionally, Fig. 4 shows the behavior of the transverse motion frequency, f_y, normalized by the natural transverse frequency in still water, f_0, whereas Fig. 5 presents the ratio between the in-line and transverse motion frequencies, f_x/f_y, as a function of the reduced velocity.

For both transverse and in-line directions, the general trend is that by decreasing the aspect ratio, the response amplitude also decreases, possibly associated with the free-end effects. By assumption, smaller immersed lengths are prone to a more three-dimensional nature of the flow downstream, presenting a decrease in the lift forces and, therefore, of the amplitude of oscillation. Another source of three-dimensional effects is the free surface due to the pierced-surface nature of the cylinder tested. In Table 2, the maximum depression L_0 of the water behind the cylinder and the maximum run-up D_1 of the water front the cylinder were evaluated as proposed by Chaplin and Teigen (2003) and Hay (1947). The value of surface elevation exceeds 15% of submerged length L only for $Fr_L > 0.5$, i.e. for tests with $L/D \leq 0.5$ and at the highest reduced velocities, in these cases the free-surface effects are summed with the free-end effects, increasing the 3D behavior of the wake. Unfortunately, these effects cannot be separated in these discussions. For tests with $Fr_L < 0.5$, the free-surface elevation is lower than 15% of the submerged length, then free-surface effects are small and can be neglected for these conditions $L/D \geq 0.5$.

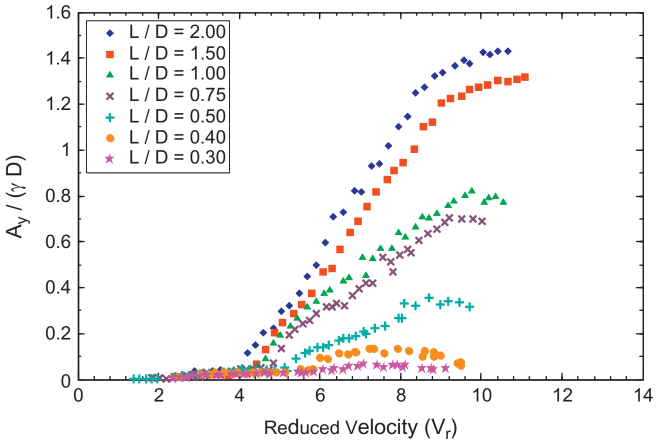

Fig. 2. Nondimensional motion amplitude in the transverse direction ($A_y/(\gamma D)$) as a function of reduced velocity (V_r) for cylinders with mass ratio of $m^* = 4.36$ and seven different aspect ratios ($L/D \leq 2.00$).

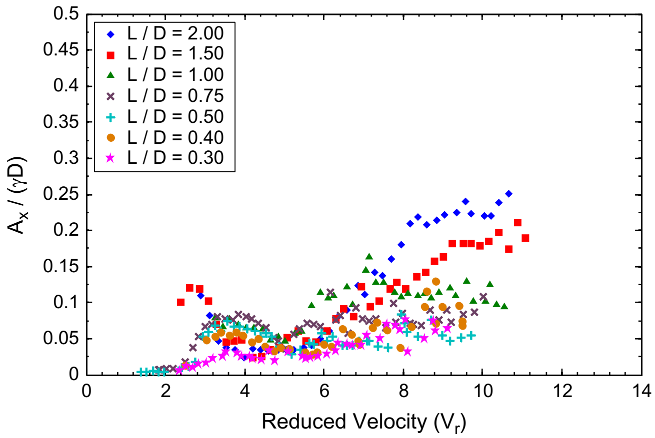

Fig. 3. Nondimensional motion amplitude in the in-line direction ($A_x/(\gamma D)$) as a function of reduced velocity (V_r) for cylinders with mass ratio of $m^* = 4.36$ and seven different aspect ratios ($L/D \leq 2.00$).

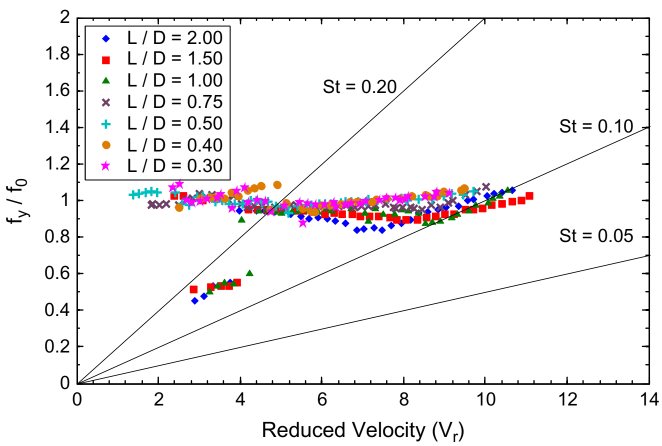

Fig. 4. Ratio between the transverse motion frequency and the natural transverse frequency in still water (f_y/f_0) as a function of reduced velocity (V_r) for cylinders with mass ratio of $m^* = 4.36$ and seven different aspect ratios ($L/D \leq 2.00$).

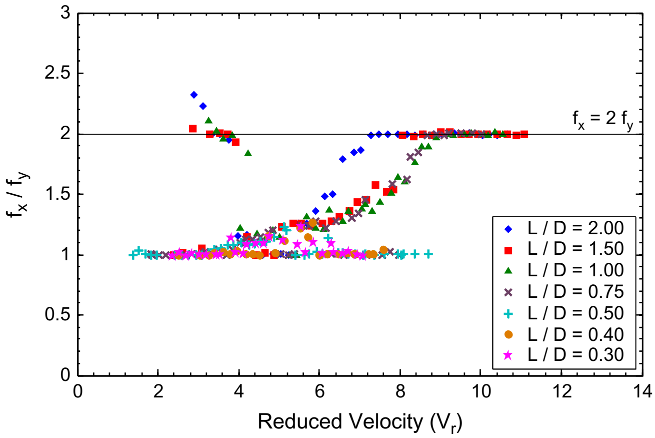

Fig. 5. Ratio between transverse and in-line motion frequencies (f_x/f_y) as a function of reduced velocity (V_r) for cylinders with mass ratio of $m^* = 4.36$ and seven different aspect ratios ($L/D \leq 2.00$).

Table 2
Parameters related with free-surface effects.

m^*	L/D	Fr_L	D_1/D	D_1/L (%)	L_0/D	L_0/L (%)
4.36	2.00	0.07–0.26	0.03	2	0.02	1
	1.50	0.07–0.32	0.05	3	0.03	2
	1.00	0.12–0.40	0.08	8	0.05	5
	0.75	0.09–0.47	0.11	15	0.06	9
	0.50	0.09–0.63	0.20	39	0.11	23
	0.40	0.20–0.74	0.27	68	0.16	39
	0.30	0.23–0.90	0.40	> 100	0.23	76
2.62	2.00	0.07–0.25	0.03	2	0.02	1
	1.00	0.09–0.40	0.08	8	0.05	5
	0.75	0.08–0.48	0.11	15	0.06	9
	0.50	0.17–0.61	0.18	37	0.11	21
1.00	2.00	0.03–0.14	0.01	1	0.01	0
	1.50	0.04–0.23	0.03	2	0.02	1

A remarkable feature observed by inspecting Fig. 2 is that there is no indication of a lower branch in any of the results. The increase of the transverse amplitudes beyond $V_r \cong 4$ is clear, with no indication of decreasing, even at reduced velocities near $V_r \cong 10$.

For cylinders with high aspect ratio, $L/D \geq 8.0$, and 2-dof, it was shown that the beginning of the lower branch is expected at $V_r \cong 8$, see e.g. Blevins and Coughran (2009), Freire and Meneghini (2010), Jauvtis and Williamson (2004), Pesce and Fujarra (2000) and Stappenbelt and Lalji (2008). However, it is important not to ignore that most of those works comprise cylinders with larger mass ratios, which can be a better explanation for the existence of the lower branch. Works by Assi et al. (2009, 2010) for cylinders with $m^*=2.0$ showed no differences between initial and upper branches, and the lower branch appeared around $V_r \cong 10$, confirming the important difference between large and small mass ratio systems.

Fig. 3 shows that the in-line amplitudes present local maxima at $V_r \cong 2.5$, followed by smaller values around reduced velocity of 5 and an increase of the peak amplitudes for larger V_r values, exactly in the same range as the peak amplitudes of the transverse direction. As well known, the in-line local peaks for $2 < V_r < 4$ are related to the resonance in this direction, according to $f_y \sim 0.5 f_0$ and $f_x \sim f_0$, consequently, $f_x/f_y \sim 2.0$; see Figs. 4 and 5. As mentioned before, Jauvtis and Williamson refer to these resonance behaviors as the in-line modes. It is noticeable, however, that such behavior is observed only for aspect ratios higher than 1.0. In other cases, the correlation seems to be not large enough to yield appreciable forces and thus motions.

The frequency results by themselves still present interesting characteristics. Firstly, Fig. 4 shows that the transverse motion frequencies remain near the natural frequency in still water for a large range of reduced velocities, $f_y/f_0 \sim 1.0$, and we see that this synchronization range is not well defined. Secondly, it is shown that only the larger aspect ratios present transverse motion frequencies equal to half the transverse natural frequency for reduced velocities lower than 4.

Again, regarding Fig. 2, it is interesting to notice that the resonance curves seem shifted to the right. From Fox and West (1993a), it is well known that the Strouhal number is highly sensitive to the aspect ratio lower than 13 diameters in length and, therefore, it is inferred that the changes in the Strouhal number are the probable reason for such a shift in the curve of peak amplitudes. If the Strouhal number is smaller, i.e. the frequency of vortex shedding is smaller, the synchronization range occurs for higher velocities that shift the amplitude curves to the right. Moreover, there is another subtle feature in the results shown in Fig. 2, namely a strong decrease of amplitudes if one compares the results for $L/D \geq 1.5$ to those for $L/D \leq 1.0$.

Perhaps the most remarkable feature of these results is the high transverse and in-line amplitudes reached by the cylinder, akin to results obtained by Jauvtis and Williamson (2004) and Stappenbelt and Lalji (2008). Those authors described the behavior of rigid cylinders elastically supported with small mass ratio and 2-dof, finding high response amplitudes of approximately 1.5*D*, for Jauvtis and Williamson associated with a "2T" mode of shedding (a triplet of vortices being formed in each half cycle). Furthermore, differently from the intermittent and weakly periodic upper branch reported in Govardhan and Williamson (2000), the so called *Super-Upper branch* is highly stable, very periodic and displays hysteretic behavior, besides presenting strong coupling between transverse and in-line movement.

The results herein presented, especially for $L/D = 1.5$ and 2.0, present high peak amplitudes in the transverse direction, reaching $A_y/(\gamma D) \cong 1.30$ and 1.40 respectively, as well as $A_x/(\gamma D) \cong 0.20$ and 0.25 for the in-line direction. This led us to believe that an analogous coupling behavior can be present, yet in our case affected by the very low aspect ratio, but not the same "2T" mode.

Respectively, Figs. 6 and 7 show the nondimensional transverse and in-line amplitudes for the cylinders with $m^* = 2.62$ and $L/D = 0.5$, 0.75, 1.0 and 2.0. Noteworthy is the mass ratio $m^* = 2.62$ adopted for the experiments discussed from Fig. 6 to Fig. 9, the same value found in Jauvtis and Williamson (2004), which helps the discussion further on.

Before that, the transverse amplitudes of motion are somewhat similar to the results presented in Fig. 2, as far as the larger amplitudes $A_y/(\gamma D) \cong 1.50$ are achieved for $L/D = 2.0$ and there is a quick decrease in amplitudes as the aspect ratio decreases, down to $A_y/(\gamma D) \cong 0.30$ for $L/D = 0.5$.

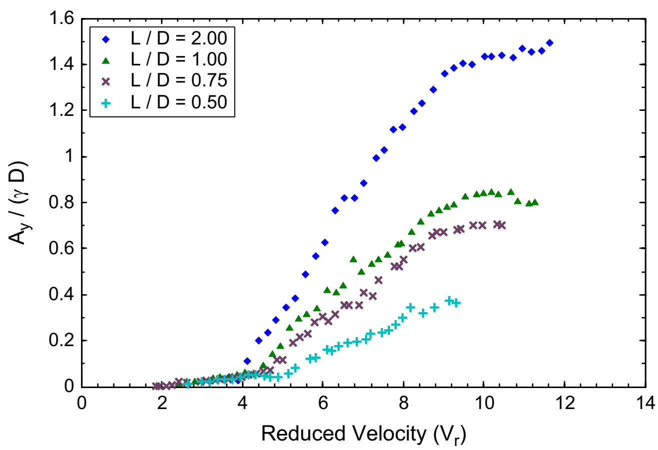

Fig. 6. Nondimensional motion amplitude in the transverse direction ($A_y/(\gamma D)$) as a function of reduced velocity (V_r) for cylinders with mass ratio of $m^* = 2.62$ and four different aspect ratios ($L/D \leq 2.00$).

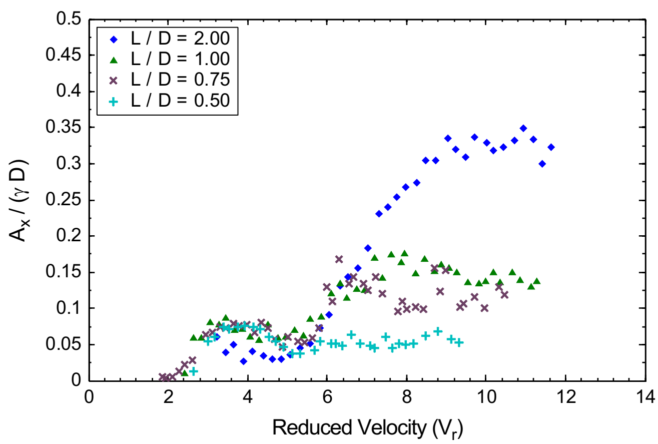

Fig. 7. Nondimensional motion amplitude in the in-line direction ($A_x/(\gamma D)$) as a function of reduced velocity (V_r) for cylinders with mass ratio of $m^* = 2.62$ and four different aspect ratios ($L/D \leq 2.00$).

However, there is some different behavior for the in-line amplitudes in which larger motions are achieved, particularly $A_x/(\gamma D) \cong 0.35$ for $L/D=2.0$, whereas for the larger mass ratio, Fig. 3, the same aspect ratio reaches values no larger than $A_x/(\gamma D) \cong 0.25$. One would expect larger in-line motion amplitudes when the mass ratio is decreased, as discussed in Jauvtis and Williamson (2004) by means of an elastically supported cylinder with $L/D=8.0$; this behavior was also observed for the shorter cylinders tested in the present work.

As in those relations between frequencies presented for the larger mass ratio, Figs. 8 and 9 present similar graphs for $m^*=2.62$. According to Fig. 9, the strong coupling between transverse and in-line motions (distinguished when $f_x/f_y \cong 2$) is present for all the aspect ratios at $V_r>7$, except for $L/D=0.5$. At the same time, by inspecting Fig. 8, one can also see that the trend in the curves more sharply follows the support lines, denoting that the "Strouhal-like" numbers are smaller.

Similarly to what was observed for the larger mass ratio, again the in-line resonance region is quite evidently within the range of $2<V_r<4$, where $f_x/f_y \cong 2$. As the reduced velocity increases, probably an initial branch is captured in $4<V_r<6$, after which coupled motions of large and stable amplitudes are observed.

Indeed, by inspecting the results in Figs. 6 and 7, one can verify three different steady regimes. The first, at a reduced velocity of 3, is featured by predominantly in-line oscillation with almost no evidence of transverse movement. On the other hand, an opposite behavior can be seen at reduced velocities of 4 and 5, clearly featured by the dominant presence of transverse oscillations. Once again, for reduced velocities higher than 6, a coupled movement starts, resulting in a notable increase of the oscillations in both directions and a ratio of two between the in-line and transverse motion frequencies, as presented in Fig. 9.

We now turn our attention to Figs. 10 and 11, where the transverse and in-line nondimensional amplitudes for $m^*=1.00$ are respectively presented for $L/D=1.5$ and 2.0; the only two possible cases under the limits given by the experimental apparatus.

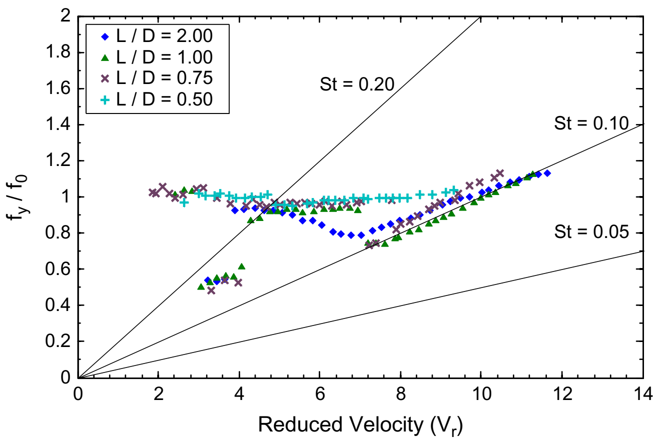

Fig. 8. Ratio between the transverse motion frequency and the natural transverse frequency in still water (f_y/f_0) as a function of reduced velocity (V_r) for cylinders with mass ratio of $m^*=2.62$ and four different aspect ratios ($L/D \le 2.00$).

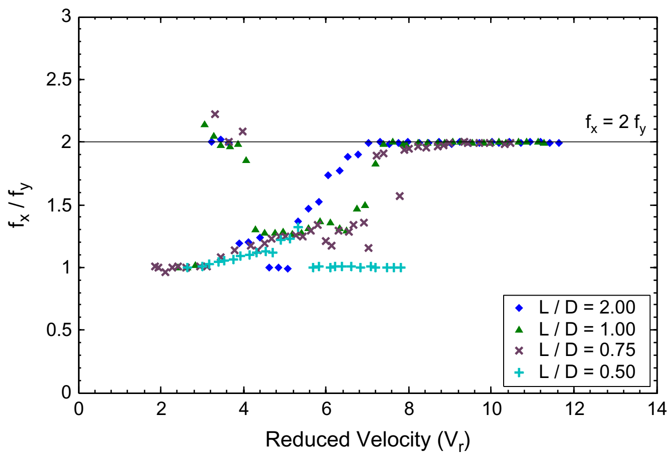

Fig. 9. Ratio between transverse and in-line motion frequencies (f_x/f_y) as a function of reduced velocity (V_r) for cylinders with mass ratio of $m^*=2.62$ and four different aspect ratios ($L/D \le 2.00$).

A small difference in terms of nondimensional amplitudes is observed as a function of the aspect ratio for $m^* = 1.00$. However, the transverse amplitudes in Fig. 10 are observed to be lower than the corresponding ones for the same aspect ratios and larger mass ratios in Figs. 2 and 6. At this point, the reason for this aspect is unclear, as one would expect larger amplitudes for such a small mass ratio, although the experiments reported in Blevins and Coughran (2009) showed the same behavior for rigid cylinders with $m^* = 1.00$, $L/D > 13.0$ and 2-dof, as compared to those from cylinders with larger mass ratio.

Conversely to what happens with the transverse motion, in the in-line direction, the amplitudes present large values around, $V_r \cong 5$. By simultaneously inspecting Figs. 10 and 11, one can identify the two resonant regimes in the in-line direction, the first related to the streamwise symmetric mode of shedding, at $1.5 \lessapprox V_r \lessapprox 2.5$, and second to the streamwise antisymmetric mode of shedding, at $2.5 \lessapprox V_r \lessapprox 4.0$. These two regimes were also observed in Nakamura et al. (2001) for short cylinder with 1-dof and further discussed in Someya et al. (2010) for short cylinders with 2-dof. After $V_r = 4$, the coupled motion takes place and the nondimensional in-line amplitudes increase gradually up to $A_x/(\gamma D) \cong 0.35$.

Fig. 12 refers to the ratio between transverse motion frequencies and the natural transverse frequency in still water, whereas Fig. 13 is related to the ratio between the in-line and transverse motion frequencies for $m^* = 1.00$. According to these graphs, most of the aspects herein reported for the cylinder with $m^* = 1.00$ are complemented by means of the behavior of nondimensional frequencies. The described in-line resonance regimes are quite evident in Fig. 12, and it is possible to observe the highly coupled motion above the reduced velocity of 5 in Fig. 13.

Vortex-shedding frequency normalized, or Strouhal frequency, seems to increase as the aspect ratio is increased for the same reduced velocity, making it possible to infer that the statement originally proposed in Okamoto and Yagita (1973) for fixed short cylinders is also valid for very short cylinders with small mass ratio and 2-dof. Naturally, this assumption takes

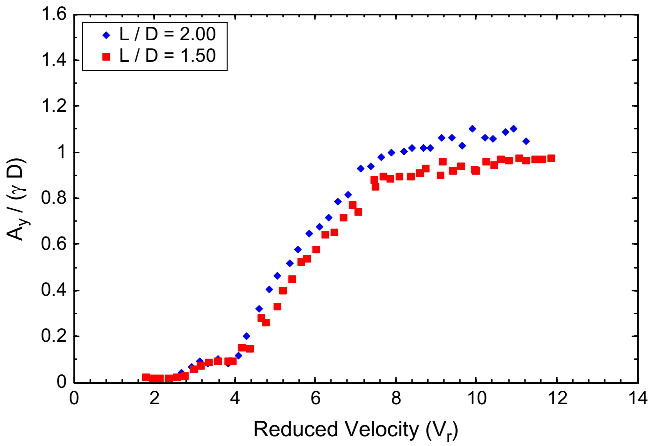

Fig. 10. Nondimensional motion amplitude in the transverse direction ($A_y/(\gamma D)$) as a function of reduced velocity (V_r) for cylinders with mass ratio of $m^* = 1.00$ and two different aspect ratios ($L/D = 1.50$ and 2.00).

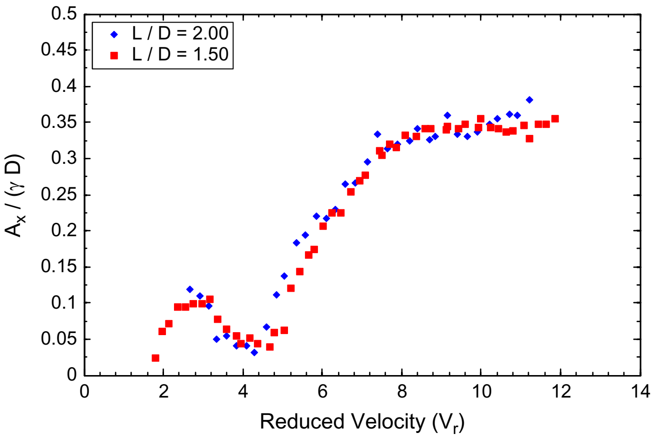

Fig. 11. Nondimensional motion amplitude in the in-line direction ($A_x/(\gamma D)$) as a function of reduced velocity (V_r) for cylinders with mass ratio of $m^* = 1.00$ and two different aspect ratios ($L/D = 1.50$ and 2.00).

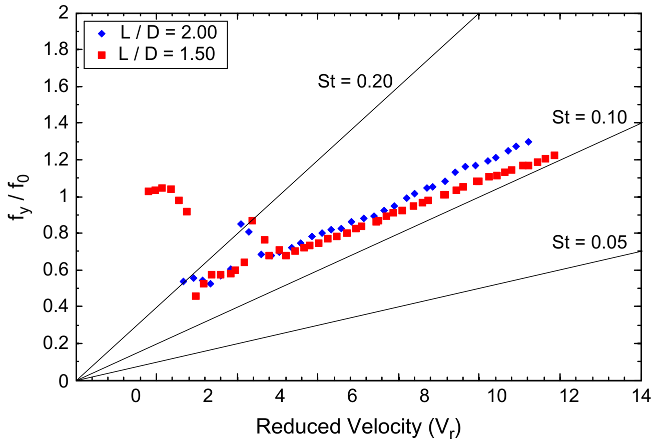

Fig. 12. Ratio between the transverse motion frequency and the natural transverse frequency in still water (f_y/f_0) as a function of reduced velocity (V_r) for cylinders with mass ratio of $m^* = 1.00$ and two different aspect ratios ($L/D = 1.50$ and 2.00).

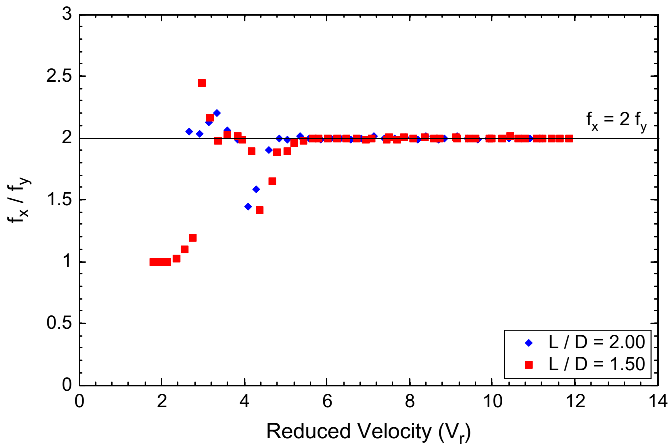

Fig. 13. Ratio between transverse and in-line motion frequencies (f_x/f_y) as a function of reduced velocity (V_r) for cylinders with mass ratio of $m^* = 1.00$ and two different aspect ratios ($L/D = 1.50$ and 2.00).

into account a transverse motion frequency approximately equal to the shedding frequency outside the synchronization region, specifically for $V_r > 5$.

It is relevant to notice that the case of $m^* = 1.00$ is highly relevant for offshore applications, as many of the floating systems present mass ratio close to unity. As shown in Gonçalves et al. (2012b), the results from fundamental studies such as the ones performed herein may be relevant to understand the behavior of more complex systems, for instance spar or monocolumn platforms. Clearly, the dynamics of floating systems is abundant in more complex aspects, especially those related to large Reynolds numbers. However, essentially speaking, it is known that the phenomenology observed in small-scales, typically characterized by low Reynolds numbers, $\mathrm{Re} < 10^5$, can be similar to what is observed in full scale, $\mathrm{Re} > 10^7$, and, in general, more conservative in terms of the parameters to be considered for the design of those systems, see for example Roddier et al. (2009). Therefore, laboratory experiments maintain their importance in such cases.

4.2. The response for fixed aspect ratio and different mass ratios

Complementary aspects gathered by the experiments are presented separately in order to better understand the influence of the mass ratio on the dynamic behavior of very short cylinders with 2-dof. Figs. 14 and 15 compare the nondimensional amplitudes for the transverse and in-line motion, respectively, both considering cylinders with $L/D = 2.0$ and mass ratios of $m^* = 4.36$; 2.62 and 1.00 These results are now organized together, so that the effect of mass ratio can be directly analyzed. Moreover, some observations are made by means of the trajectories on the XY-plane, the *Lissajous* figures.

By comparing the results in Fig. 14, it can be stated that the dynamic responses for the cylinders with mass ratios equal to 4.36 and 2.62 are quite similar. The same cannot be said for the dynamic responses of a cylinder with $m^* = 1.00$.

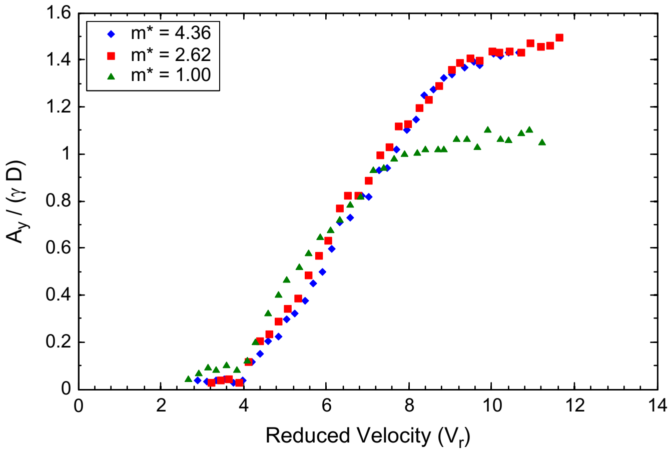

Fig. 14. Nondimensional motion amplitude in the transverse direction ($A_y/(\gamma D)$) as a function of reduced velocity (V_r) for cylinders with $L/D = 2.00$ and three different small mass ratios ($m^* \le 4.36$).

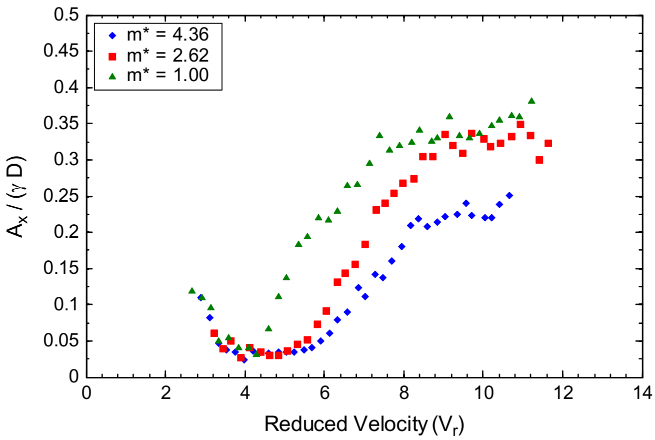

Fig. 15. Nondimensional motion amplitude in the in-line direction ($A_x/(\gamma D)$) as a function of reduced velocity (V_r) for cylinders with $L/D = 2.00$ and three different small mass ratios ($m^* \le 4.36$).

The behavior of smaller peak amplitudes for the smaller mass ratio is emphasized in Fig. 14, as pointed out in Blevins and Coughran (2009). It is interesting to notice for the in-line amplitudes, Fig. 15, that the higher amplitudes do correspond to the smaller mass ratio, $m^* = 1.00$.

Considering the frequency results in Figs. 16 and 17, the distinct behavior for the results from the smaller mass ratio is much more interesting, since the frequency ratio f_y/f_0 in Fig. 16 does not reach the unit frequency ratio as the other results. Instead, as of $V_r \cong 4.5$, this ratio increases linearly according to a larger coefficient. The same behavior was reported in Dahl et al. (2006, 2010) for systems with $f_{0x} \sim f_{0y}$. Moreover, one notices in Fig. 17 that the coupled motion, identified by $f_x/f_y = 2.0$, takes place much earlier than in the other mass ratios.

For the cylinder with $m^* = 1.00$, the coupling between in-line and transverse oscillations appears early at $V_r \cong 5.0$, condition preserved for values up to at least a reduced velocity of 10. Those aspects seem to indicate a different behavior of fluid-structural interaction; unfortunately, full understanding can be achieved only by means of flow measurements or visualizations, as well as qualitatively by numerical simulations. Research approaches in this direction are in progress.

Fig. 18 presents the trajectories in the *XY*-plane, *Lissajous* figures. Firstly, one notices that the onset of transverse motions is $V_r > 5$ in all cases. As commented before, the cases for $m^* = 2.62$ and 4.36 reach extremely high transverse amplitudes of $A_y/(\gamma D) \cong 1.50$. On the other hand, the case of $m^* = 1.00$, instead, presents lower transverse but higher in-line amplitudes. Such a behavior starts even at relatively low reduced velocities. Such differences are clearly observed by comparing the trajectories in Fig. 18, particularly at $V_r \cong 7$, when, for the $m^* = 1.00$ case, the *8-shape* trajectories become very well defined. What would be the cause for such an unexpected behavior? In fact, 1-dof experiments are characterized by presenting larger transverse amplitudes as lower is the mass ratio, m^*. The proper answer might be related to the energy transferring process, from the steady stream to the oscillatory hydroelastic system, composed by the elastically

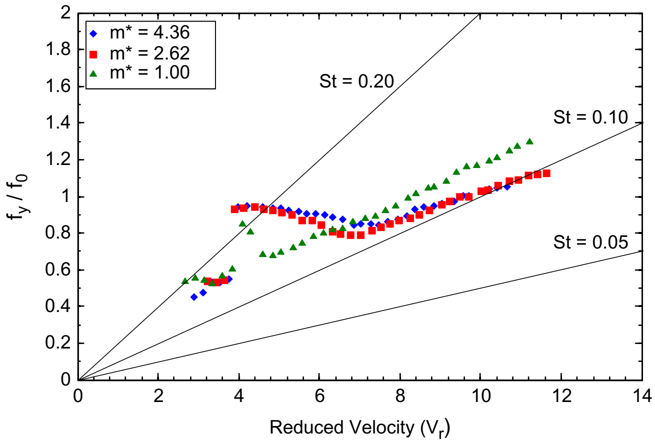

Fig. 16. Ratio between the transverse motion frequency and the natural transverse frequency in still water (f_y/f_0) as a function of reduced velocity (V_r) for cylinders with $L/D=2.00$ and three different small mass ratios ($m^*\leq 4.36$).

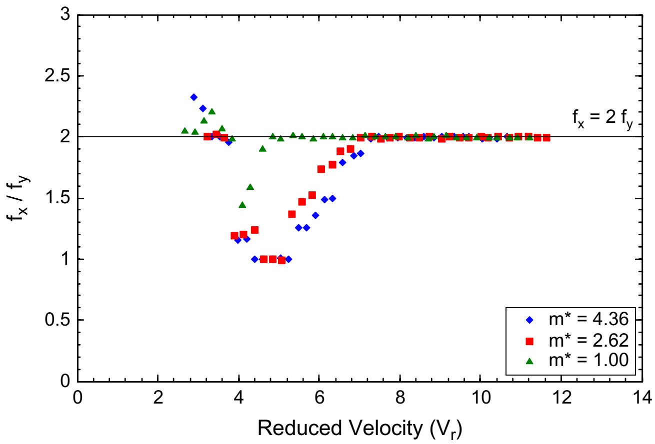

Fig. 17. Ratio between transverse and in-line motion frequencies (f_x/f_y) as a function of reduced velocity (V_r) for cylinders with $L/D=2.00$ and three different small mass ratios ($m^*\leq 4.36$).

mounted cylinder and the wake. In fact, as it will be shown next, at a given reduced velocity, the total amount of transferred energy from the steady stream may be inferred as practically invariant with respect to m^*.

Such a conjecture is outlined as follows. Consider the instantaneous kinetic energy T of the hydroelastic system—the elastically mounted cylinder and the wake. As usual, the oscillatory part of the kinetic energy related to the fluid is usually written by considering a proper definition for the added mass, such that:

$$T=\frac{1}{2}(m_s+m_{ax}){U_x}^2+\frac{1}{2}(m_s+m_{ay}){U_y}^2, \tag{1}$$

where m_{ax} and m_{ay} are, respectively, the added mass in the transverse and in-line directions and U_x and U_y are the corresponding components of the cylinder velocity.

Proceeding, the velocity amplitude in the transverse direction can be approximately evaluated as

$$U_y=\frac{A_y}{\gamma}(2\pi f_y), \tag{2}$$

where f_y is the dominant frequency of oscillation in that direction; or, alternatively, in a nondimensional form as

$$V_y=\frac{U_y}{f_0 D}, \tag{3}$$

$$V_y=2\pi\frac{A_y}{\gamma D}\frac{f_y}{f_0}. \tag{4}$$

The same procedure can be applied to the nondimensional velocity in the in-line direction, recalling that, depending on the mass ratio, the dominant frequency may be double or equal the dominant frequency in the transverse direction. On the

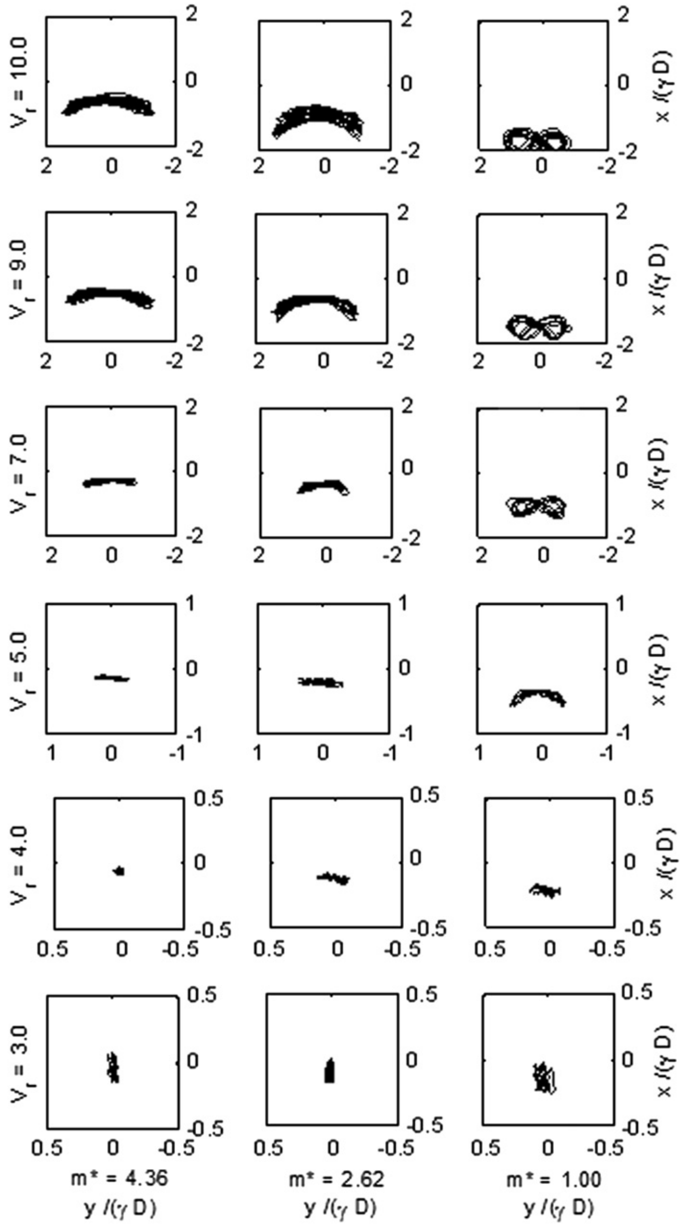

Fig. 18. Trajectories on the *XY*-plane, Lissajous figures, as a function of reduced velocity (V_r) for three different small mass ratio cylinders ($m^* \leq 4.36$) and low aspect ratio $L/D = 2.00$.

other hand, mass and added mass can be written in the nondimensional form as

$$m^* = \frac{m_s}{m_d}, \tag{5}$$

$$m_a^* = \frac{m_a}{m_d}. \tag{6}$$

Eq. (1) is then written in nondimensional form:

$$\frac{T}{m_d(f_0 D)^2} = \frac{1}{2}(m^* + m_{ax}^*){V_x}^2 + \frac{1}{2}(m^* + m_{ay}^*){V_y}^2. \tag{7}$$

Notice that this form may be regarded as a nondimensional measure of the mechanical energy of the oscillatory system. The experimental results were transformed, according to (7) and plotted in Fig. 19 as function of the reduced velocity. The result is weakly sensitive to the reduced mass parameter. It appears that the energy transferring process, from the steady stream to the oscillatory system is, as conjectured, almost invariant with respect the reduced mass for the same aspect ratio.

For each particular reduced velocity value, V_r, the nondimensional mechanical energy of the system is about the same, for all three mass ratio values tested. In other words, at small reduced mass values, the in-line oscillation 'drains' energy from the transverse oscillation, what explains why the amplitude of transverse oscillation decreases.

The added mass coefficients for in-line and transverse directions as a function of reduced velocity are presented in Figs. 20 and 21, respectively. These coefficients were calculated from the indirect measurement of total hydrodynamic force, in the in-line and transverse directions, inferred as proposed in Jauvtis and Williamson (2004):

$$m_s\ddot{x}+c\dot{x}+k_x x=F_{Hx}, \tag{8}$$

$$m_s\ddot{y}+c\dot{y}+k_y y=F_{Hy}, \tag{9}$$

where c is the structural damping of the system and F_H is the total hydrodynamic force acting on the system. The structural damping ratio for the tests is $\zeta_s=0.1$, which allows neglecting the structural damping force component. Considering, as usual, that the component of the total hydrodynamic force in phase with the acceleration is related to the added mass, it is possible to evaluate the added mass coefficient at the characteristic frequency of the motion, from a standard frequency domain analysis, as proposed by Fujarra and Pesce (2002). For the motions in the transverse direction:

$$m^*_{ay}(f_y)=\frac{-\mathcal{R}\{\mathcal{F}[F_{Hy}]/\mathcal{F}[\ddot{y}]\}}{m_d}, \tag{10}$$

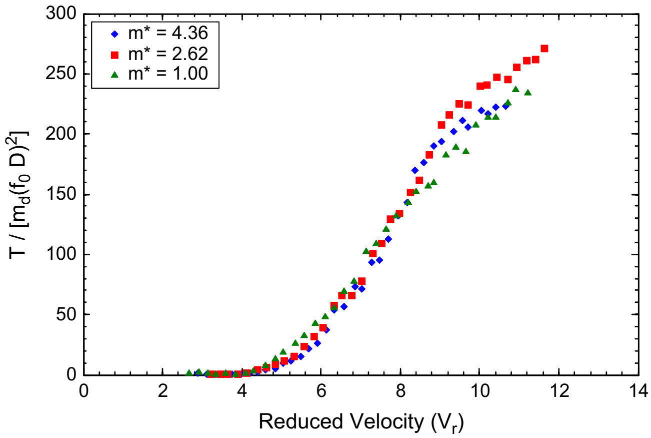

Fig. 19. Nondimensional maximum instantaneous kinetic energy of the hydroelastic system as a function of reduced velocity (V_r) for cylinders with $L/D=2.00$ and three different small mass ratios ($m^*\leq 4.36$).

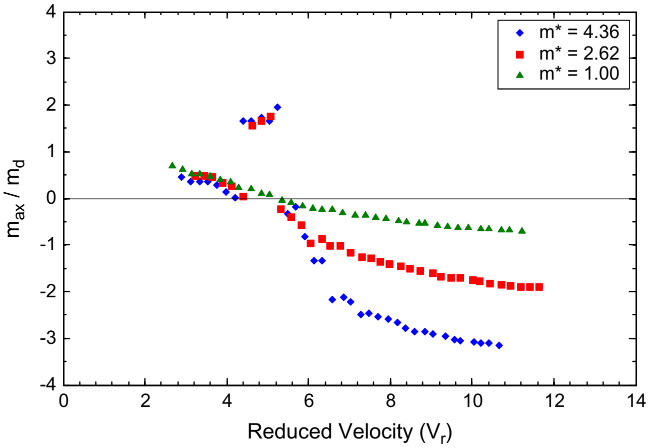

Fig. 20. Nondimensional added mass coefficient in the in-line direction (m^*_{ax}) as a function of reduced velocity (V_r) for cylinders with $L/D=2.00$ and three different small mass ratios ($m^*\leq 4.36$).

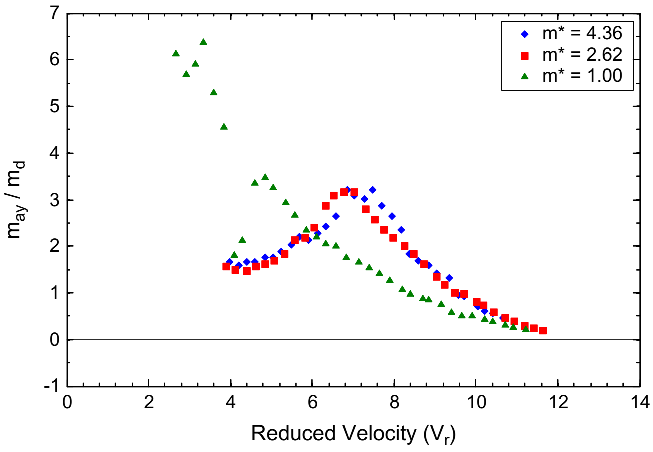

Fig. 21. Nondimensional added mass coefficient in the transverse direction (m^*_{ay}) as a function of reduced velocity (V_r) for cylinders with $L/D = 2.00$ and three different small mass ratios ($m^* \leq 4.36$).

Table 3
"Strouhal-like" numbers for cylinders with $m^*=1.00$.

L/D	**St**	R^2
2.0	0.0985	0.9968
1.75	0.0894	0.9832
1.5	0.0824	0.9990

where $\mathcal{R}[\square]$ is the real part of a complex number and $\mathcal{F}[\square]$ is the Fourier transform operator. The same procedure is applied for the motions in the in-line direction. The added mass can also be evaluated in time domain, as proposed in Vikestad et al. (2000), leading to similar results, as exemplified in Fujarra and Pesce (2002).

The added mass results for the in-line direction, in Fig. 20, showed a decrease with increasing reduced velocity with asymptotic value of $m^*_{ax} = -m^*$, the same behavior reported in Cunha et al. (2006) and Jauvtis and Williamson (2004). The zero crossing occurred for all cases around $V_r \approx 4$, which confirms the resonance of the in-line motion around this reduced velocity. However, the added mass results for the transverse direction, Fig. 21, did not present the zero crossing regions, confirming the absence of the lower branch for the present experiments,. On the other hand, added mass results for high aspect ratio cylinders, as in Vikestad et al. (2000), usually show a zero crossing where the lower branch appears and the resonance process is finished. In fact, as pointed out in Cunha et al. (2006), the zero-crossing phenomenon is a characteristic of going through a resonance, as is the asymptotic trend, far away from the resonance point.

Through the trajectories in the *XY*-plane, one can also verify larger offsets in the in-line direction for the case of $m^* = 1.00$, possibly related to a strong dynamic amplification of the drag forces. The dynamic amplification corresponds to a large increase in the drag loads due to the transverse motion, which means that the transverse motion reinforces the mean drag load. In Gonçalves et al. (2012b), it is shown that the mean drag coefficient increases from approximately 0.70 up to 1.10, due to the dynamic amplification present in the dynamic behavior of cylinders with very low aspect ratio and small mass ratio.

Another interesting comparison can be made between the trajectories for our results with $m^* = 2.62$ and the results for the similar mass ratio in Jauvtis and Williamson (2004). From that comparison, we observe the in-line resonance for $m^* < 3.00$. However, in our case, it is not clear if the anti-symmetric resonance is actually present, as the transverse amplitudes are very low in that region. For $V_r \cong 5$, the transverse motions are clearer and for $V_r \cong 7$ the coupled motions are present. For $V_r \cong 10$, the *8-shape* figure from the results of Jauvtis and Williamson is more deformed, indicating that the motions might not be well correlated and an imminent drop of the amplitudes is likely, turning to the lower branch. This possibility could not be analyzed in our experiments due to the limitations of our apparatus.

Finally, we should further comment the results presented in Table 3, which show the calculated "Strouhal-like" numbers. For the case of fixed mass ratio, $m^* = 1.00$, and different aspect ratios, one notices that the "Strouhal-like" numbers decrease for decreasing aspect ratios, as also observed for free-oscillating cylinders in Gonçalves et al. (in press), Morse et al. (2008) and Stappenbelt and Lalji (2008) and, for fixed cylinders, in Fox and Apelt (1993a), Norberg (1994), Okamoto and Yagita (1973) and Sakamoto and Arie (1983).

4.3. Investigating the relation between aspect ratio and mass ratio

The dependency of the in-line and transverse amplitudes regarding the mass ratio and aspect ratio parameters is further investigated with the graphs in Figs. 22 and 23. In the former, the ratio between in-line and transverse amplitudes, A_x/A_y, is depicted as a function of the reduced velocity for cylinders of different aspect ratios and $m^* = 4.36$, whereas in the latter, the same ratio between amplitudes is presented for cylinders with a fixed aspect ratio of 2.00 and those three mass ratios tested.

In Fig. 22, one notices the scatter of points for $V_r < 4$. This range corresponds to the in-line resonance region, for which the transverse amplitudes are very small, yielding somewhat scattered results without a clear trend. However, for larger reduced velocities, i.e. $V_r > 4$ and particularly for aspect ratios larger than 0.50, the ratio between in-line and transverse amplitudes find a limit around $A_x/A_y \approx 0.15$.

Perhaps, a more interesting aspect can be identified by inspecting Fig. 23, which shows that the ratios between amplitudes tend to asymptotic values depending on the mass ratio, $A_x/A_y \cong 0.33$; 0.23 and 0.17 respectively for $m^* = 4.36$; 2.62 and 1.00, as a clear consequence of the strong coupling between in-line and transverse motions, featured by ratios between amplitudes of smaller values, as well as the increased mass ratio.

Figs. 24 and 25 respectively show the maximum transverse and in-line motion amplitudes for different aspect ratios and mass ratios. They clearly show that the amplitudes decrease with decreasing aspect ratios, as already discussed. Nevertheless, the counter-intuitive result is the one from the lowest mass ratio, $m^* = 1.00$, in which the maximum transverse amplitudes are lower than the ones with larger mass ratios, as discussed before.

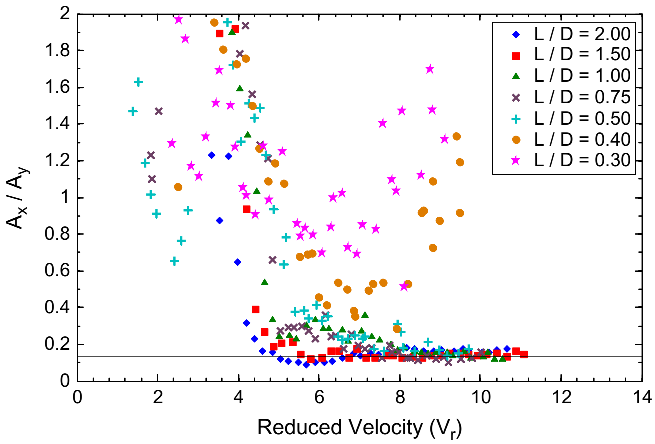

Fig. 22. Ratio between in-line and tranverse amplitudes of oscillation (A_x/A_y) as a function of reduced velocity (V_r) for cylinders with mass ratio of $m^* = 4.36$ and seven different aspect ratios ($L/D \le 2.00$).

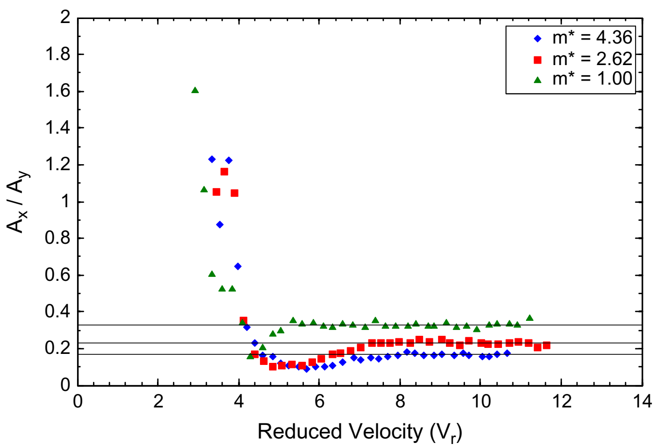

Fig. 23. Ratio between in-line and tranverse amplitudes of oscillation (A_x/A_y) as a function of reduced velocity (V_r) for cylinder with aspect ratio of $L/D = 2.00$ and three different mass ratios ($m^* \le 4.36$).

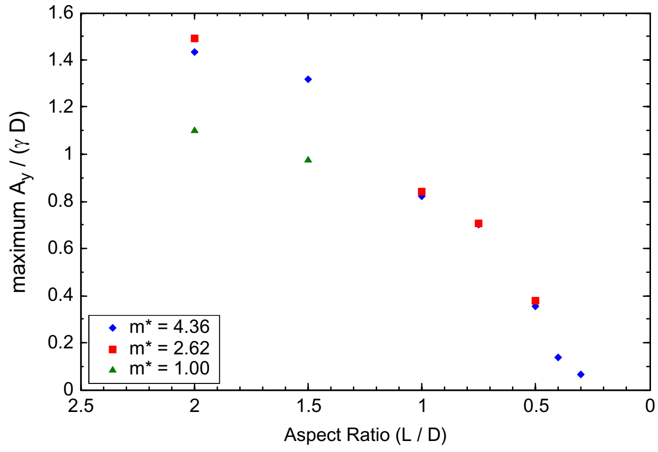

Fig. 24. Maximum nondimensional amplitude in the transverse direction ($A_y/(\gamma D)$) as a function of the aspect ratio (L/D) for cylinders with three different mass ratios ($m^* \leq 4.36$).

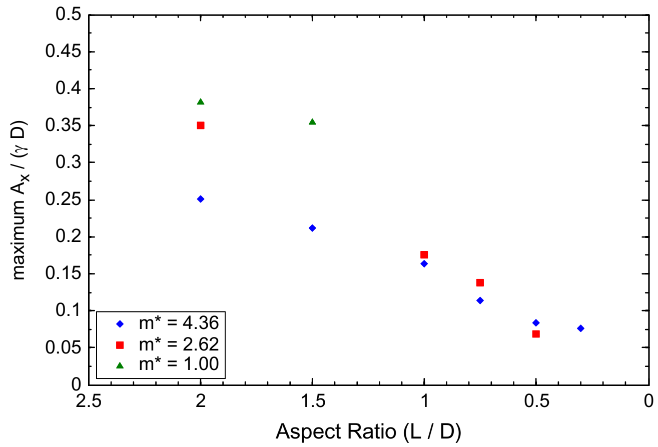

Fig. 25. Maximum nondimensional amplitude in the in-line direction ($A_x/(\gamma D)$) as a function of aspect ratio (L/D) for three different small mass ratio cylinders ($m^* \leq 4.36$).

5. Conclusion

Response amplitudes and frequencies due to the VIV phenomenon on a circular cylinder with two degrees of freedom were measured for three different mass ratios and very low aspect ratios ranging from $L/D{=}0.3$ up to $L/D{=}2.0$. The experiments were carried out in a recirculating water channel with Reynolds numbers in the subcritical regime of $6000 < \text{Re} < 70\,000$. In spite of such very low aspect ratios, large response amplitudes were observed, comparable to those observed for VIV of "infinite cylinders". This behavior is directly related to the freedom to oscillate in both directions, in-line and transversely to the fluid flow. Even for the short cylinders with different mass ratios, the influence of aspect ratio was quite important and was found to have a most striking effect on the transverse amplitudes, being considerably smaller when the aspect ratio was decreased. In the lowest aspect ratio cases $L/D \leq 0.5$ in the highest reduced velocities, the Froude number based on the cylinder submerged length becomes large $\text{Fr}_L > 0.5$ and the free-surface effects can be strong inserting more three-dimensional structures on the wake beyond the one inserted by the free-end effects. As a result of the large motions recorded in the in-line direction, a strong coupling with the transverse motions was identified for aspect ratios greater than 0.75 and $m^* = 4.36$, visibly featured by in-line motion frequencies twice the transversal ones, $f_x/f_y \cong 2$, as well as by the trajectories in the *XY*-plane. The *Lissajous* figures are particularly interesting for the case with $m^* = 1.00$ and $L/D{=}2.0$, where *8-shape* trajectories are quite evident.

Definitely, the most interesting aspect was identified for the cases of $m^* = 1.00$, because of its smaller transverse amplitudes compared to those for the same aspect ratio and larger mass ratios. This counter-intuitive behavior was assigned to the large motions in the in-line direction, occurring earlier in terms of reduced velocity. In fact, a simple assumption of a roughly similar energy amount spent by the cylinder (or equivalently, work done by the cylinder) in one cycle of coupled movement at each reduced velocity could be the explanation for the smaller transverse amplitudes in the case of unitary mass ratio, since part of the total energy is simultaneously spent with larger motions in the in-line direction. Moreover, independently of its nature, the cases of $m^* = 1.00$ and $L/D \geq 0.4$ are noteworthy, which still present transverse amplitudes greater than one diameter and, consequently, are highly relevant for offshore applications, where many of the floating systems definitely have aspect ratios close to those values, e.g. spars and monocolumn platforms. Moreover, the decrease of the "Strouhal-like" number as the aspect ratio is decreased seems to indicate another reason for the large amplitudes at higher reduced velocities, with no evidence of a lower branch, at least up to $V_r = 12$.

Finally, the fundamental results presented here may be relevant to understand the behavior of more complex systems, for instance spar or monocolumn platforms, although the dynamics of floating systems have more complex aspects, amongst which the strong dependence on the Reynolds number. Essentially speaking, however, it is known that the phenomenology recognized in small-scale, typically characterized by lower Reynolds numbers, is similar to that observed in full scale and, in general, more conservative in terms of the parameters to be considered for the design of those systems. Therefore, we believe that laboratory experiments still constitute an important activity in such cases.

Further works can be done to better understand the wake downstream the low aspect ratio cylinders using PIV and force measurements. Another way to improve understanding is to provide CFD simulations of the same conditions carried out in this work and also for fixed cylinder. Researches along these lines are being conducted by the group.

Acknowledgments

The authors would like to acknowledge FAPESP, CAPES and CNPq for the financial support. Prof. Fujarra expresses his gratitude to the support provided by the Brazilian Navy and by the Maritime Research Institute Netherlands during his sabbatical year, period in which this work was completed. The authors are also grateful to Dr. Ivan Korkischko and César Freire for his support during the experimental set up, as well as to Ingrid Wolfs and Jaap de Wilde for their valuable support to this text. Finally, the authors especially thank Prof. Celso Pesce for his invaluable contributions to the discussions on added mass and energy balance, in Section 4.2.

References

Adaramola, M.S., Akinlade, O.G., Sumner, D., Bergstrom, D.J., Schenstead, A.J., 2006. Turbulent wake of a finite circular cylinder of small aspect ratio. Journal of Fluids and Structures 22, 919–928.
Assi, G.R.S., Meneghini, J.R., Aranha, J.A.P., Bearman, P.W., Casaprima, E., 2006. Experimental investigation of flow-induced vibration interference between two circular cylinders. Journal of Fluids and Structures 22, 819–827.
Assi, G.R.S., Bearman, P.W., Kitney, N., 2009. Low drag solutions for suppressing vortex-induced vibration of circular cylinders. Journal of Fluids and Structures 25, 666–675.
Assi, G.R.S., Bearman, P.W., Kitney, N., Tognarelli, M.A., 2010. Suppression of wake-induced vibration of tandem cylinders with free-to-rotate control plates. Journal of Fluids and Structures 26, 1045–1057.
Ayoub, A., Karamcheti, K., 1982. An experiment on the flow past a finite circular cylinder at high subcritical and supercritical Reynolds numbers. Journal of Fluid Mechanics . 118, 1–26.
Baban, F., So, R.M.C., 1991a. Aspect ratio effect on flow-induced forces on circular cylinders in a cross-flow. Experiments in Fluids 10, 313–321.
Baban, F., So, R.M.C., 1991b. Recirculating flow behind and unsteady forces on finite-span circular cylinders in a cross-flow. Journal of Fluids and Structures 5, 185–206.
Blevins, R.D., 1990. Flow-induced Vibration. Krieger, Malabar, FL.
Blevins, R.D., Coughran, C.S., 2009. Experimental investigation of vortex-induced vibration in one and two dimensions with variable mass, damping, and Reynolds number. Journal of Fluids Engineering 131 (10), 101202.
Chaplin, J.R., Teigen, P., 2003. Steady flow past a vertical surface-piercing circular cylinder. Journal of Fluids and Structures 18, 271–285.
Cunha, L.D., Pesce, C.P., Wanderley, J.B.V., Fujarra, A.L.C., 2006. The robustness of the added mass in VIV models. In: Proceedings of the 25th International Conference on Offshore Mechanics and Arctic Engineering. OMAE Paper 92323, Hamburg, Germany, USA.
Dahl, J.M., Hover, F.S., Triantafyllou, M.S., 2006. Two-degree-of-freedom vortex-induced vibrations using a force assisted apparatus. Journal of Fluids and Structures 22, 807–818.
Dahl, J.M., Hover, F.S., Triantafyllou, M.S., Dong, S., Karniadakis, G.E., 2007. Resonant vibrations of bluff bodies cause multivortex shedding and high frequency forces. Physical Review Letters 99, 144503.
Dahl, J.M., Hover, F.S., Triantafyllou, M.S., Oakley, O.H., 2010. Dual resonance in vortex-induced vibrations at subcritical and supercritical Reynolds numbers. Journal of Fluid Mechanics 643, 395–424.
Farivar, D., 1981. Turbulent uniform flow around cylinders of finite length. AIAA Journal 19 (3), 275–281.
Fox, T.A., Apelt, C.J., 1993. Fluid-induced loading of cantilevered circular cylinders in a low-turbulence uniform flow. Part 3: fluctuating loads with aspect ratios 4 to 25. Journal of Fluids and Structures 7, 375–386.
Fox, T.A., West, G.S., 1993a. Fluid-induced loading of cantilevered circular cylinders in a low turbulence uniform flow. Part 1: mean loading with aspect ratios in the range 4 to 30. Journal of Fluids and Structures 7, 1–14.
Fox, T.A., West, G.S., 1993b. Fluid-induced loading of cantilevered circular cylinders in a low-turbulence uniform flow. Part 2: fluctuating loads on a cantilever of aspect ratio 30. Journal of Fluids and Structures 7, 15–28.
Franzini, G.R., Pereira, A.A.P., Fujarra, A.L.C., Pesce, C.P., 2008. Experiments of VIV under frequency modulation and at constant Reynolds number. In: Proceedings of the 27th International Conference on Offshore Mechanics and Arctic Engineering, OMAE Paper 57957. Estoril, Portugal.
Franzini, G.R., Gonçalves, R.T., Fujarra, A.L.C., Meneghini, J.R., 2010. Experiments of VIV on rigid and inclined cylinders mounted on a base with two degrees-of-freedom. In: Proceedings of the BBVIV-6 Bluff Body Wakes and Vortex-Induced Vibrations. Capri Island, Italy.
Franzini, G.R., Pesce, C.P., Gonçalves, R.T., Fujarra, A.L.C., Pereira, A.A.P., 2011. Analysis of multimodal vortex-induced vibrations using the Hilbert–Huang spectral analysis. In: Proceedings of the 3rd International Conference on Hilbert–Huang Transformation: Theory and Applications. Qingdao, China.
Freire, C.M., Meneghini, J.R., 2010. Experimental investigation of VIV on a circular cylinder mounted on an articulated elastic base with two degrees-of-freedom. In: Proceedings of the BBVIV-6 Bluff Body Wakes and Vortex-Induced Vibrations. Capri Island, Italy.
Fujarra, A.L.C., Pesce, C.P., 2002. Added mass of an elastically mounted cylinder in water subjected to vortex-induced vibrations. In: Proceedings of the 21st International Conference on Offshore Mechanics and Arctic Engineering, OMAE Paper 28375. Oslo, Norway.
Gonçalves, R.T., Franzini, G.R., Fujarra, A.L.C., Meneghini, J.R., 2010a. Two degrees-of-freedom vortex-induced vibration of a circular cylinder with low aspect ratio. In: Proceedings of the BBVIV-6 Bluff Body Wakes and Vortex-Induced Vibrations. Capri Island, Italy.

Gonçalves, R.T., Fujarra, A.L.C., Rosetti, G.F., Nishimoto, K., 2010b. Mitigation of vortex-induced motion (VIM) on a monocolumn platform: forces and movements. Journal of Offshore Mechanics and Arctic Engineering 132 (4), 041102.
Gonçalves, R.T., Franzini, G.R., Rosetti, G.F., Fujarra, A.L.C., Nishimoto, K., 2012a. Analysis methodology for vortex-induced motion (VIM) on a monocolumn platform applying the Hilbert–Huang transform method. Journal of Offshore Mechanics and Arctic Engineering 134 (1), 011103.
Gonçalves, R.T., Rosetti, G.F., Fujarra, A.L.C., Freire, C.M., Franzini, G.R., Meneghini, J.R., 2012b. Experimental comparison of two degrees-of-freedom vortex-induced vibration on high and low aspect ratio cylinders with small mass ratio. Journal of Vibration and Acoustics, 134 (1), 061009.
Govardhan, R.N., Williamson, C.H.K., 2000. Modes of vortex formation and frequency response of a freely vibrating cylinder. Journal of Fluid Mechanics 420, 85–130.
Hay, A.D., 1947. Flow About Semi-submerged Cylinders With Finite Length. Princeton University Report, Princeton, NJ.
Huang, N.E., Shen, Z., Long, S.R., Wu, M.C., Shin, H.H., Zheng, Q., Yen, N.C., Tung, C.C., Liu, H.H., 1998. The empirical mode decomposition and the Hilbert spectrum for nonlinear and non-stationary time series analysis. Proceedings of the Royal Society of London A 454, 903–995.
Iungo, G.V., Pii, L.M., Buresti, G., 2012. Experimental investigation on the aerodynamic loads and wake flow features of a low aspect-ratio circular cylinder. Journal of Fluids and Structures 28, 279–291.
Jauvtis, N., Williamson, C.H.K., 2003. Vortex-induced vibration of a cylinder with two degrees of freedom. Journal of Fluids and Structures 17, 1035–1042.
Jauvtis, N., Williamson, C.H.K., 2004. The effect of two degrees of freedom on vortex-induced vibration at low mass and damping. Journal of Fluid Mechanics 509, 23–62.
Kawamura, T., Hiwada, M., Hibino, T., Mabuchi, I., Kumada, M., 1984. Flow around a finite circular cylinder on a flat plate. Bulletin of the Japan Society of Mechanical Engineers 27 (232), 2142–2151.
King, R., 1974. Vortex excited structural oscillations of a circular cylinder in steady currents. In: Proceedings of the 6th Annual Offshore Technology Conference, OTC Paper 1948. Houston, TX, USA.
Morse, T.L., Govardhan, R.N., Williamson, C.H.K., 2008. The effect of end conditions on vortex-induced vibration of cylinders. Journal of Fluids and Structures 24, 1227–1239.
Nakamura, A.O., Okajima, A., Kosugi, T., 2001. Experiments on flow-induced in-line oscillation of a circular cylinder in a water tunnel. JSME International Journal: Series B 44 (4), 705–711.
Norberg, C., 1994. An experimental investigation of the flow around a circular cylinder: influence of aspect ratio. Journal of Fluid Mechanics 258, 287–316.
Okamoto, T., Yagita, M., 1973. The experimental investigation on the flow past circular cylinder of finite length placed normal to the plane surface in a uniform stream. Bulletin of the Japan Society of Mechanical Engineers 16 (95), 805–814.
Palau-Salvador, G., Stoesser, T., Fröhlich, J., Kappler, M., Rodi, W., 2010. Large eddy simulations and experiments of flow around finite-height cylinders. Flow Turbulence Combust 84, 239–275.
Park, C.W., Lee, S.J., 2000. Free end effects on the near wake flow structure behind a finite circular cylinder. Journal of Wind Engineering and Industrial Aerodynamics 88, 231–246.
Pesce, C.P., Fujarra, A.L.C., 2000. Vortex-induced vibrations and jump phenomenon: experiments with a clamped flexible cylinder in water. International Journal of Offshore and Polar Engineering 10 (1), 26–33.
Pesce, C.P., Fujarra, A.L.C., Kubota, L.K., 2006. The Hilbert–Huang spectral analysis method applied to VIV. In: Proceedings of the 25th International Conference on Offshore Mechanics and Arctic Engineering, OMAE Paper 92119. Hamburg, Germany.
Roddier, D., Finnigan, T., Liapis, S., 2009. Influence of the Reynolds number on spar Vortex Induced Motions (VIM): multiple scale model test comparisons. In: Proceedings of the 28th International Conference on Ocean, Offshore and Arctic Engineering, OMAE Paper 79991. Honolulu, Hawaii, USA.
Rödiger, T., Knauss, H., Gaisbauer, U., Krämer, E., 2007. Pressure and heat flux measurements on the surface of a low-aspect-ratio circular cylinder mounted on a ground plate. New Results in Numerical and Experimental Fluid Mechanics VI 96, 121–128.
Roh, S.C., Park, S.O., 2003. Vortical flow over the free end surface of finite circular cylinder mounted on a flat plate. Experiments in Fluids 34, 63–67.
Rostamy, N., Sumner, D., Bergstrom, D.J., Bugg, J.D., 2012. Local flow field of a surface-mounted finite circular cylinder. Journal of Fluids and Structures 34, 105–122.
Sakamoto, H., Arie, M., 1983. Vortex shedding from a rectangular prism and circular cylinder placed vertically in a turbulent boundary layer. Journal of Fluid Mechanics 126, 147–165.
Sanchis, A., Sælevik, G., Grue, J., 2008. Two-degree-of-freedom vortex-induced vibrations of a spring-mounted rigid cylinder with low mass ratio. Journal of Fluids and Structures 24, 907–919.
Sanchis, A., 2009. Two degrees of freedom vortex-induced vibrations of a rigid circular cylinder with varying natural frequencies in the X and Y directions. In: Proceedings of the 28th International Conference on Ocean, Offshore and Arctic Engineering, OMAE Paper 80252. Honolulu, Hawaii, USA.
Sarpkaya, T., 1996. Vorticity, Free Surface and Surfactants. Annual Review of Fluid Mechanics 28, 83–128.
Silveira, L.M.Y., Martins, C.A., Cunha, L.D., Pesce, C.P., 2007. An investigation on the effect of tension variation on VIV of risers. In: Proceedings of the 26th International Conference on Offshore Mechanics and Arctic Engineering, OMAE Paper 29247. San Diego, USA.
Someya, S., Kuwabara, J., Li, Y., Okamoto, K., 2010. Experimental investigation of a flow-induced oscillating cylinder with two degrees-of-freedom. Nuclear Engineering and Design 240, 4001–4007.
Stappenbelt, B., Lalji, F., 2008. Vortex-induced vibration super-upper response branch boundaries. International Journal of Offshore and Polar Engineering 18 (2), 99–105.
Sumner, D., Heseltine, J.L., Dansereau, O.J.P., 2004. Wake structure of a finite circular cylinder of small aspect ratio. Experiments in Fluids 37, 720–730.
Vikestad, K., Vandiver, J.K., Larsen, C.M., 2000. Added mass and oscillation frequency for a circular cylinder subjected to vortex-induced vibrations and external disturbance. Journal of Fluids and Structures 14, 1071–1088.
Williamson, C.H.K., Jauvtis, N., 2004. A High-amplitude 2t mode of vortex-induced vibration for a light body in XY motion. European Journal of Mechanics B/Fluids 23, 107–114.